Path Generation, Path Following and Coordinated Control for Time-Critical Missions of Multiple UAVs

I. Kaminer,* O. Yakimenko,* A. Pascoal,** and R. Ghabcheloo**

Abstract — **The paper proposes a solution to the problem of coordinated control of multiple unmanned air vehicle (UAV) to ensure collision-free maneuvers under strict spatial and temporal constraints. First, a set of feasible trajectories are generated for all UAVs using a new direct method of optimal control that takes into account rules for collision avoidance. A by-product of this step yields, for each vehicle, a spatial path to be followed together with a nominal desired speed profile. Each vehicle is then made to execute a pure path following maneuver in three-dimensional space by resorting to a novel 3D algorithm. Finally, the speed profile for each vehicle is adjusted to enforce the temporal constraints that must be met in order to coordinate the fleet of vehicles. Simulations illustrate the potential of the methodology developed.**

Keywords: Unmanned Air Vehicles, Coordinated Motion Control, Trajectory Generation, Path Following, Graph Theory.

I. INTRODUCTION

This paper addresses the problem of coordinated control of multiple unmanned air vehicles (UAVs) under tight spatial and temporal constraints. This topic of research is motivated by the need to develop strategies for coordinated ground target suppression and sequential auto-landing for multiple UAVs. Both mission scenarios require a group of UAVs to execute time-critical maneuvers in close proximity of each other. For the case of ground target suppression, a formation of UAVs must break up and execute a coordinated maneuver to arrive at a predefined position over the target at a given time. Similarly, for the case of sequential autolanding, a formation must also break up and arrive at the assigned glideslope point separated by pre-specified safe-guarding time intervals. A key requirement underlying these missions is that all maneuvers be collision-free.

In recent years, there has been widespread interest in the problem of coordinated motion control of fleets of autonomous vehicles. Applications include aircraft and spacecraft formation flying [1]-[4], coordinated control of land robots [5]-[6], and control of multiple surface and underwater vehicles [7]-[10]. The work reported in the literature addresses a large class of topics that include, among others, leader/follower formation flying, control of the center of mass and radius of dispersion of swarms of vehicles, and uniform coverage of an area by a group of surveying robots. There are however applications with UAVs that do not fit the scenarios commonly described in the literature. Namely, the missions described in the present work that include spatial as well as temporal requirements.

To deal with the new scenarios, a methodology for coordinated control of UAVs is proposed that unfolds in three basic steps. First, a set of feasible trajectories are generated for all UAVs using a direct method of optimal control that takes explicitly into account the boundary initial and final conditions, the simplified UAV dynamics, and safety rules for collision avoidance. This is done by resorting to an extension of the work reported in [11] to multiple UAVs. A by-product of this step yields - for each vehicle - a spatial path to be followed, together with a desired nominal speed profile along that path. The second step consists of making each vehicle execute a path following maneuver along its assigned path by resorting to a new nonlinear path following algorithm in three dimensional space that generalizes the one introduced in [5] for wheeled robots. Finally, the speed profile of each vehicle is adjusted to enforce the temporal constraints that must be met in order to coordinate the fleet of vehicles. Clearly, the methodology proposed relies on the decoupling of space and time in the problem formulation. The rationale for this procedure stems from the fact that path following controllers are easier to design than trajectory tracking controllers and, when properly designed, yield smooth approaching maneuvers to the spatial curves that must be tracked. At the same time, this strategy will naturally generate the control activity that is required for each vehicle to capture its nominal path generated during the path planning phase, even if due to unforeseen disturbances the vehicle deviates too much from it.

The paper is organized as follows. Section II describes the methodology adopted for real-time, feasible UAV trajectory generation. Section III offers a solution to the problem of path following in 3D. Section IV addresses the coordination of a fleet of AUVs in time. Finally, Section V includes the results of simulations with the nonlinear dynamic models of a small fleet of UAVs.

II. FEASIBLE TRAJECTORY GENERATION

This section describes an algorithm for multiple UAV real-time trajectory generation that is based on the results reported in [11-14] for a single aircraft. The new algorithm developed allow for the computation of feasible trajectories for multiple UAVs that are de-conflicted in space and which can be tracked by resorting to the path following algorithm described in Section III.

In what follows we denote by $\mathbf{p}_c(\tau) := \left[x_c(\tau), y_c(\tau), z_c(\tau)\right]^T$ a desired trajectory to be followed by a single UAV, parameterized by some parameter, say the virtual arc $\tau \in \left[0; \tau_f\right]$, where τ_f is the

* Dept. of Mechanical and Astronautical Engineering, Naval Postgraduate School, Monterey, CA, USA.
** Institute for Systems and Robotics (ISR) and Dept. Electrical Engineering and Computers, Instituto Superior Técnico (IST), Lisbon, Portugal.

total virtual arc length that for our purposes we view as an optimization parameter. We assume that the coordinates $x_c(\tau)$, $y_c(\tau)$, $z_c(\tau)$ can be represented by algebraic polynomials of degree N of the form

$$x_i(\tau) = \sum_{k=0}^{N} a_{ik}\tau^k \ , \ i = 1,2,3 \qquad (1)$$

where, for notational convenience, we set x_1=x, x_2=y, and x_3=z. The degree N of the polynomials $x_i(\tau)$ is determined by the number of boundary conditions that must be satisfied. Let d_0 and d_f be the highest-order of the derivatives of $x_i(\tau)$ that must meet specified boundary constraints at the initial and final points of a trajectory, respectively. Then, the minimum degree N* of each polynomial in (1) is $N^* = d_0 + d_f + 1$. For example, if the desired trajectory includes constraints on initial and final positions, velocities and accelerations (second-order derivatives) then the degree of each polynomial is N*=2+2+1=5. Additional degrees of freedom may be included by making $N > N^*$. As an illustrative example, Table 1 shows how to compute the polynomial coefficients in (1) for 5th and 6th order polynomial trajectories. The second column differs from the first one in that fictitious initial jerk constraints are included. This increases the order of the resulting polynomial but affords extra optimization (design) parameters x'''_{i0}; $i = 1,2,3$. Figure 1a shows examples of admissible 5th-order polynomial trajectories when the optimization parameter τ_f is varied (all boundary constraints are satisfied by default, but there is no control over the higher-order derivatives: $x'''_{i0} := 6a_{i3}$, $x'''_{if} = \sum_{k=3}^{N} a_{ik}\frac{k!}{(k-3)!}\tau_f^{k-3}$, $i = 1,2,3$). Figure 1b shows how an increase in the number of optimization parameters leads to a larger class of admissible trajectories (in this particular case we acquire control over the initial jerk). It is important to point out that the parameterization (1) completely determines the UAV's spatial profile, i.e. a 3D trajectory that satisfies all boundary conditions by construction.

Table 1. Examples of computation of the coefficients of polynomial trajectories.

Boundary conditions	x_{i0} , x'_{i0} , x''_{i0} , x_{if} , x'_{if} , x''_{if}	
d_0/d_f	2/2	3 (adding fictitious jerk x'''_{i0})/2
N*/N	5/5	5/6
Linear algebraic matrix equation to solve for the coefficients a_{ik}	$\begin{pmatrix} 1 & 0 & 0 & 0 & 0 & 0 \\ 0 & 1 & 0 & 0 & 0 & 0 \\ 0 & 0 & 2 & 0 & 0 & 0 \\ 1 & \tau_f & \tau_f^2 & \tau_f^3 & \tau_f^4 & \tau_f^5 \\ 0 & 1 & 2\tau_f & 3\tau_f^2 & 4\tau_f^3 & 5\tau_f^4 \\ 0 & 0 & 2 & 6\tau_f & 12\tau_f^2 & 20\tau_f^3 \end{pmatrix} \begin{pmatrix} a_{i0} \\ a_{i1} \\ a_{i2} \\ a_{i3} \\ a_{i4} \\ a_{i5} \end{pmatrix} = \begin{pmatrix} x_{i0} \\ x'_{i0} \\ x''_{i0} \\ x_{if} \\ x'_{if} \\ x''_{if} \end{pmatrix}$	$\begin{pmatrix} 1 & 0 & 0 & 0 & 0 & 0 & 0 \\ 0 & 1 & 0 & 0 & 0 & 0 & 0 \\ 0 & 0 & 2 & 0 & 0 & 0 & 0 \\ 0 & 0 & 0 & 6 & 0 & 0 & 0 \\ 1 & \tau_f & \tau_f^2 & \tau_f^3 & \tau_f^4 & \tau_f^5 & \tau_f^6 \\ 0 & 1 & 2\tau_f & 3\tau_f^2 & 4\tau_f^3 & 5\tau_f^4 & 6\tau_f^5 \\ 0 & 0 & 2 & 6\tau_f & 12\tau_f^2 & 20\tau_f^3 & 30\tau_f^4 \end{pmatrix} \begin{pmatrix} a_{i0} \\ a_{i1} \\ a_{i2} \\ a_{i3} \\ a_{i4} \\ a_{i5} \\ a_{i6} \end{pmatrix} = \begin{pmatrix} x_{i0} \\ x'_{i0} \\ x''_{i0} \\ x'''_{i0} \\ x_{if} \\ x'_{if} \\ x''_{if} \end{pmatrix}$

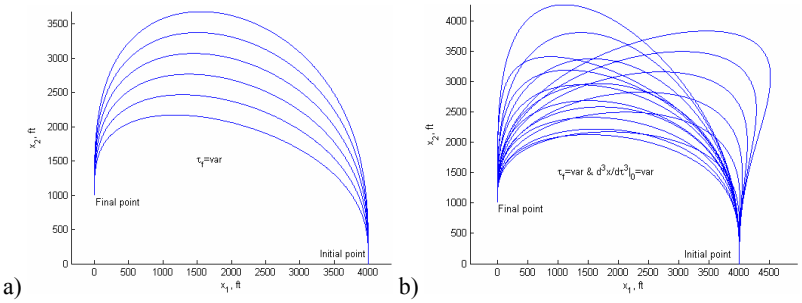

a) b)

Figure 1. Admissible trajectories for 5th (a) and 6th (b) order polynomials with a single (τ_f) and multiple (τ_f and x'''_{i0},; $i = 1,2,3$) optimization parameters, respectively.

The fact that the virtual arc was selected as a parameter in (1) allows for additional flexibility. If $\tau := t$, then defining spatial profiles means defining speed profiles along a trajectory as well. This is due to the fact that vehicle speed is related to the time derivatives of the trajectory coordinates as

$$v(t) = \sqrt{\dot{x}_1^2(t) + \dot{x}_2^2(t) + \dot{x}_3^2(t)} \ . \qquad (2)$$

Figure 2 shows the speed profiles corresponding to trajectories in Fig.1 for the case of $\tau := t$. This figure also demonstrates that increasing the number of optimization parameters allows one to obtain speed profiles that do not exceed predefined constraints.

A feasible trajectory is one that can be tracked by an UAV without having it exceed predefined bounds on the velocity $v(t)$ along the corresponding path as well as on the total acceleration. Let $v_{\min}$, $v_{\max}$ and $a_{\max}$ denote predefined

bounds on the velocity and total acceleration, respectively. Further define $\lambda(\tau)=\frac{d\tau}{dt}$. Then, from (2) we obtain

$$v(\tau)=\lambda(\tau)\sqrt{x_1'^2(\tau)+x_2'^2(\tau)+x_3'^2(\tau)}=\lambda(\tau)\left\|p_c'(\tau)\right\|. \quad (3)$$

Notice that $\lambda(\tau)$ can be chosen as a polynomial of a degree sufficiently high to satisfy boundary conditions on speed. Then, a trajectory $p_c(\tau)$ is *feasible* if

$$v_{\min}\le\lambda(\tau)\left\|p_c'(\tau)\right\|\le v_{\max}\text{, and}$$

$$\left\|p_c''(\tau)\lambda^2(\tau)+p_c'(\tau)\lambda'(\tau)\lambda(\tau)\right\|\le a_{\max},\ \forall\tau\in\left[0,\tau_f\right]. \quad (4)$$

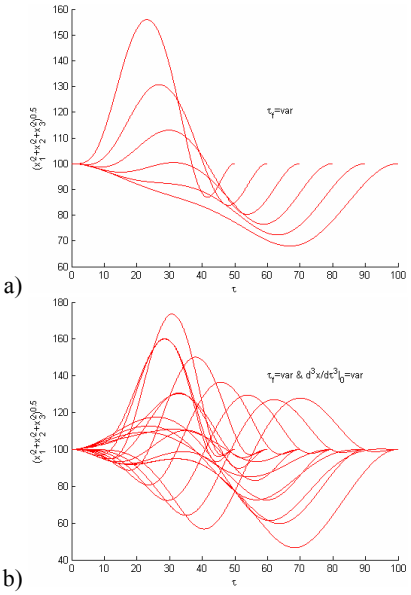

Figure 2. Speed profiles corresponding to trajectories shown on Fig.1 in case $\tau:=t$.

Let Ξ be the vector of optimization parameters: τ_f, x_{i0}''', $i=1,...,3$ and polynomial coefficients defining $\lambda(\tau)$. A feasible trajectory can be obtained by solving, for example, the following optimization problem

$$F1:\ \begin{cases}\min\limits_{\Xi}\tau_f\\ \textit{subject to (4)}\end{cases}$$

For the case of multiple UAVs, say n, the dimension of the problem increases. To guarantee spatial deconfliction, one set of constraints may be added to account for a minimum separation distance E between each pair of vehicles. Let τ_{fi} denote the total path length of the i^{th} UAV and let $w_i>0$. Feasible, spatially deconflicted trajectories for each vehicle can thus be obtained by solving the optimization problem

$$F2:\ \begin{cases}\min\limits_{\Xi_i,i=1,n}\sum\limits_{i=1,n}w_i\tau_{fi}\\ \textit{subject to (4) for each } i\in[1,n] \textit{ and}\\ \min\limits_{\substack{j,k=1,...,n\\ j\neq k}}\left\|p_c^j(\tau_j)-p_c^k(\tau_k)\right\|^2\ge E^2,\forall(\tau_j,\tau_k)\in[0,\tau_{fj}]\times[0,\tau_{fk}]\end{cases}$$

The optimization problems *F1, F2* can be effectively solved in real-time by adding a penalty function G as discussed in [11] and by using any zero-order method.

As an example, Fig.3 illustrates the flexibility afforded by the reference polynomials to compute a coordinated target suppression mission by three UAVs (moving from right to left).

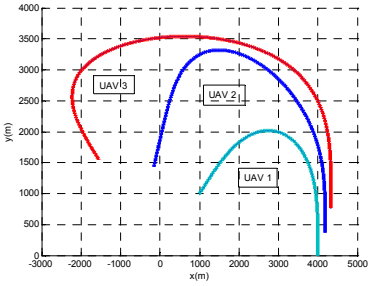

Fig.3. Coordinated attack trajectories.

III. PATH FOLLOWING OF POLYNOMIAL TRAJECTORIES

The algorithm for trajectory generation introduced in Section II yields - for each vehicle - a spatial path to be followed, together with the corresponding nominal speed profile. To follow the paths computed, this section describes a path following algorithm that extends that in [5] to a 3D setting and introduces a further modification aimed at meeting time-critical inter-vehicle constraints. At this level, only the simplified kinematic equations of the vehicle will be addressed by taking pitch rate and yaw rated as virtual outer-loop control inputs. The dynamics can be dealt with at a later stage by introducing an inner-loop control law. However, this will not be analyzed formally in the paper.

The notation required is introduced next, with reference to Fig.4. Let *{F}* a Serret-Frenet frame attached to a generic point on the path and let *{W}* be the wind frame attached to the UAV (a frame that has its *x*-axis aligned with the UAV's velocity vector). Further let ${}^F\omega_{FI}$ denote the angular velocity of *{F}* with respect to inertial frame *{I}*, resolved in *{F}*. Denote by $p_c(\tau)$, where τ denotes the arc length introduced in previous section, the path to be followed and by Q denote the center of mass of the aircraft. Let P be an arbitrary point on the path that plays the role of the center of mass of a "virtual" aircraft to be followed. This is in contrast with the set-up for path following originally proposed in [15] where P was simply defined as the point on the path that is closest to the vehicle. Since this point may not be uniquely defined, the strategy in [15] led to very conservative estimates for the region of attraction about the path to be followed. Endowing P with an extra degree of freedom (that will be exploited later) is the key to the algorithm presented in [5] that is extended in this paper to the 3D case. Notice that Q can be resolved in *{I}* as $q_I=\begin{bmatrix}x & y & z\end{bmatrix}^T$ or in *{F}* as $q_F=\begin{bmatrix}s_1 & y_1 & z_1\end{bmatrix}^T$. With the above notation, the simplified UAV kinematic equations can be written as

$$\begin{cases} \dot{x} = v\cos\gamma\cos\psi \\ \dot{y} = -v\cos\gamma\sin\psi \\ \dot{z} = v\sin\gamma \\ \begin{bmatrix}\dot{\gamma}\\ \dot{\psi}\end{bmatrix} = \begin{bmatrix}1 & 0\\ 0 & \cos^{-1}\gamma\end{bmatrix}\begin{bmatrix}q\\ r\end{bmatrix} \end{cases} \tag{5}$$

where v is the magnitude of the UAV's velocity vector, γ is the flight path angle, ψ is the heading angle, and and r are the y-axis and z-axis components, respectively of the vehicle's rotational velocity resolved in wind frame $\{W\}$. With a slight abuse of notation, q and r will be often referred to as pitch rate and yaw rate, respectively in the wind frame $\{W\}$.

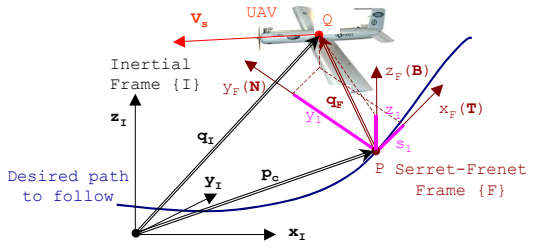

Fig.4. Problem geometry.

Remark 1. – In the kinematic model (5), q and r play the role of virtual control inputs. Clearly, the dynamics of the UAV are not taken into consideration at this level. This is in line with the control strategies adopted in a vast number of flight control systems with an inner-outer (dynamic-kinematic) loop configuration. In these cases, a controller is available to stabilize the inner loop and to track the angular rate commands issued by the outer loop. We therefore concentrate on the design of the outer (kinematic) loop. However, a complete inner-outer setup is used in Section V to drive a full 6DOF nonlinear model of an UAV.

Following standard nomenclature [16]-[17],

$$T(\tau) := \frac{dp(\tau)}{d\tau}\Big/\left\|\frac{dp(\tau)}{d\tau}\right\|,\ N(\tau) := \frac{dT(\tau)}{d\tau}\Big/\left\|\frac{dT(\tau)}{d\tau}\right\| \text{ and}$$

$$B(\tau) = T(\tau)\times N(\tau)$$

denote the tangent, normal, and binormal, respectively to the path at the point determined by τ. The vectors T, N, B are orthonormal and define the basis vectors of $\{F\}$ as well as the rotation matrix ${}^I_F R = [T\ N\ B]$. from $\{F\}$ to $\{I\}$. It is well known that ${}^F\omega_{FI} = \begin{bmatrix}\varsigma\dot{\tau} & 0 & \kappa\dot{\tau}\end{bmatrix}^T$, where $\kappa(\tau) := \left\|\frac{dT(\tau)}{d\tau}\right\|$ is the curvature of $P_c(\tau)$ and $\varsigma(\tau) := \left\|\frac{dB(\tau)}{d\tau}\right\|$ is its torsion.

With the notation above (see also Fig.4)

$$q_I = p_c(\tau) + {}^I_F R q_F, \tag{6}$$

and therefore

$$\dot{q}_I = {}^I_F R\begin{bmatrix}\dot{\tau}\\ 0\\ 0\end{bmatrix} + {}^I_F R\begin{bmatrix}\dot{s}_1\\ \dot{y}_1\\ \dot{z}_1\end{bmatrix} + {}^I_F R\left({}^F\omega_{FI}\times\begin{bmatrix}\dot{s}_1\\ \dot{y}_1\\ \dot{z}_1\end{bmatrix}\right) \tag{7}$$

$$\Rightarrow$$

$${}^F_I R\begin{bmatrix}\dot{x}\\ \dot{y}\\ \dot{z}\end{bmatrix} = \begin{bmatrix}\dot{\tau}(1-\kappa y_1)+\dot{s}_1\\ \dot{y}_1 + \dot{\tau}(\kappa s_1 - \varsigma z_1)\\ \dot{z}_1 + \varsigma\dot{s}y_1\end{bmatrix} \tag{8}$$

$$\Rightarrow$$

$$\begin{bmatrix}\dot{s}_1\\ \dot{y}_1\\ \dot{z}_1\end{bmatrix} = \begin{bmatrix}-\dot{\tau}(1-\kappa y_1)\\ -\dot{\tau}(\kappa s_1 - \varsigma z_1)\\ -\varsigma\dot{\tau}y_1\end{bmatrix} + {}^F_W R\begin{bmatrix}v\\ 0\\ 0\end{bmatrix}, \tag{9}$$

where we used the fact that

$${}^F_I R\begin{bmatrix}\dot{x}\\ \dot{y}\\ \dot{z}\end{bmatrix} = {}^F_W R\,{}^W_I R\begin{bmatrix}\dot{x}\\ \dot{y}\\ \dot{z}\end{bmatrix} = {}^F_W R\begin{bmatrix}v\\ 0\\ 0\end{bmatrix}. \tag{10}$$

Let λ_e denote the Euler angles ϕ_e, θ_e, ψ_e that parameterize locally the rotation matrix from $\{F\}$ to $\{W\}$. Then, $\dot{\lambda}_e = Q^{-1}(\lambda_e)\,{}^W\omega_{WF}$, where

$$Q^{-1}(\lambda_e) = \begin{bmatrix}1 & \sin\phi_e\tan\theta_e & \cos\phi_e\tan\theta_e\\ 0 & \cos\phi_e & -\sin\phi_e\\ 0 & \dfrac{\sin\phi_e}{\cos\theta_e} & \dfrac{\cos\phi_e}{\cos\theta_e}\end{bmatrix} \tag{11}$$

is nonsingular for $\theta_e \neq \pm\frac{\pi}{2}$ and ${}^W\omega_{WF}$ denotes the angular velocity of $\{W\}$ with respect to $\{F\}$ resolved in $\{W\}$. Note that ${}^W\omega_{WF} = {}^W\omega_{WI} - {}^W\omega_{FI}$ and ${}^W\omega_{FI} = {}^W_F R\,{}^F\omega_{FI}$. Therefore,

$$\dot{\lambda}_e = Q^{-1}(\lambda_e)\left({}^W\omega_{WI} - {}^W_F R(\lambda_e)\,{}^F\omega_{FI}\right) \tag{12}$$

and

$$\begin{bmatrix}\dot{\theta}_e\\ \dot{\psi}_e\end{bmatrix} = \begin{bmatrix}\sin\psi_e\varsigma\dot{\tau}\\ -\dot{\tau}\left(\varsigma\tan\theta_e\cos\psi_e + \kappa\right)\end{bmatrix} + \begin{bmatrix}\cos\phi_e & -\sin\phi_e\\ \dfrac{\sin\phi_e}{\cos\theta_e} & \dfrac{\cos\phi_e}{\cos\theta_e}\end{bmatrix}\begin{bmatrix}q\\ r\end{bmatrix} =: D + G\begin{bmatrix}q\\ r\end{bmatrix}. \tag{13}$$

where D and G are defined for all $\theta_e \neq \pm\frac{\pi}{2}$. Let

$$\begin{bmatrix}q\\ r\end{bmatrix} = G^{-1}\left\{\begin{bmatrix}u_\theta\\ u_\psi\end{bmatrix} - D\right\}. \tag{14}$$

Then, combining equations (9) and (14) yields the equations for the (path following) error dynamics:

$$G_e = \begin{cases} \dot{s}_1 = -\dot{\tau}(1-\kappa y_1) + v\cos\theta_e\cos\psi_e \\ \dot{y}_1 = -\dot{\tau}(\kappa s_1 - \varsigma z_1) + v\cos\theta_e\sin\psi_e \\ \dot{z}_1 = -\varsigma\dot{\tau}y_1 - v\sin\theta_e \\ \dot{\theta}_e = u_\theta \\ \dot{\psi}_e = u_\psi \end{cases} \tag{15}$$

Notice how the rate of progression $d\tau/dt$ of point P along the path becomes an extra variable that can be manipulated at will. With the above notation, the path following problem can now be formulated in a rigorous manner. The objectives are to drive the center of the mass of the UAV to P and to

align its total velocity with the tangent to the path at that point. A similar formulation was used in [18] to address path following for mobile robots.

Problem 1 (Path Following) *Given a spatially defined polynomial path* $p_c(\tau)$ *(see Section II) and a velocity profile* $v(t) > 0$, $\forall t \geq 0$, *determine feedback control laws for* q, r *and* $\dot{\tau}$ *to drive the linear errors* s_1, y_1 *and* z_1 *and the rotational errors* θ_e, ψ_e *asymptotically to zero.*

A solution to the above path following problem is presented below.

Proposition 1. *Consider the kinematic equations of an UAV given in (5) and let* $p_c(\tau)$ *be a path to be followed. Suppose the speed v(t) of the UAV satisfies* $v(t) > v_{\min}, \forall t \geq 0$. *Define* $\delta_\theta = \sin^{-1}\left(\theta_a \frac{z_1}{|z_1| + d_1}\right)$ *and* $\delta_\psi = \sin^{-1}\left(\psi_a \frac{y_1}{|y_1| + d_2}\right)$ *for some* $1 \geq \theta_a > 0, 1 \geq \psi_a > 0, d_1 > 0$ *and* $d_2 > 0$. *Then the feedback control laws*

$$\begin{aligned}
\dot{\tau} &= K_1 s_1 + v\cos\theta_e \cos\psi_e \\
u_\theta &= -K_2(\theta_e - \delta_\theta) + \frac{c_2}{c_1} z_1 v \frac{\sin\theta_e - \sin\delta_\theta}{\theta_e - \delta_\theta} + \dot{\delta}_\theta \\
u_\psi &= -K_3(\psi_e - \delta_\psi) - \frac{c_3}{c_1} y_1 v\cos\theta_e \frac{\sin\psi_e - \sin\delta_\psi}{\psi_e - \delta_\psi} + \dot{\delta}_\psi,
\end{aligned} \tag{16}$$

with $K_1 > 0, K_2 > 0, K_3 > 0$ *drive* s_1, y_1 *and* z_1, *together with* θ_e, ψ_e *asymptotically to zero.*

Proof. Consider a candidate Lyapunov function

$$V = \frac{1}{2c_1}(s_1^2 + y_1^2 + z_1^2) + \frac{1}{2c_2}(\theta_e - \delta_\theta)^2 + \frac{1}{2c_3}(\psi_e - \delta_\psi)^2,$$

for some $c_1 > 0$, $, c_2 > 0$ and $, c_3 > 0$ Notice how the Lyapunov function captures the deviations of the translational errors from zero and those of the rotational errors from the desired values of δ_θ and δ_ψ. The latter should be viewed as "desired approach angles" aimed at shaping the transient phase of the approach to the path. Their choice is inspired by previous work of Samson et al. [15] on path following for wheeled robots. Computing the time-derivative of *V* yields

$$\begin{aligned}
\dot{V} &= \frac{s_1\dot{s}_1}{c_1} + \frac{y_1\dot{y}_1}{c_1} + \frac{z_1\dot{z}_1}{c_1} + \frac{\theta_e - \delta_\theta}{c_2}(\dot{\theta}_e - \dot{\delta}_\theta) + \frac{\psi_e - \delta_\psi}{c_3}(\dot{\psi}_e - \dot{\delta}_\psi) \\
&= \frac{s_1}{c_1}(-\dot{\tau}(1 - \kappa y_1) + v\cos\theta_e\cos\psi_e) + \frac{y_1}{c_1}(-\dot{\tau}(\kappa s_1 - \varsigma z_1) + v\cos\theta_e\sin\psi_e) + \frac{z_1}{c_1}(-\varsigma\dot{\tau} y_1 - v\sin\theta_e) \\
&+ \frac{\theta_e - \delta_\theta}{c_2}(u_\theta - \dot{\delta}_\theta) + \frac{\psi_e - \delta_\psi}{c_3}(u_\psi - \dot{\delta}_\psi) = \frac{s_1}{c_1}(-\dot{\tau} + v\cos\theta_e\cos\psi_e) + \frac{y_1}{c_1} v\cos\theta_e\sin\psi_e - \frac{z_1}{c_1} v\sin\theta_e \\
&+ \frac{\theta_e - \delta_\theta}{c_2}(u_\theta - \dot{\delta}_\theta) + \frac{\psi_e - \delta_\psi}{c_3}(u_\psi - \dot{\delta}_\psi) + \frac{y_1}{c_1} v\cos\theta_e\sin\delta_\psi - \frac{y_1}{c_1} v\cos\theta_e\sin\delta_\psi - \frac{z_1}{c_1} v\sin\delta_\theta + \frac{z_1}{c_1} v\sin\delta_\theta
\end{aligned} \tag{17}$$

Let $\dot{\tau}$, u_θ and u_ψ be defined by (16). Then

$$\begin{aligned}
\dot{V} &= -K_1\frac{s_1^2}{c_1} - K_2\frac{(\theta_e - \delta_\theta)^2}{c_2} - K_3\frac{(\psi_e - \delta_\psi)^2}{c_3} + \frac{y_1}{c_1} v\cos\theta_e\sin\delta_\psi - \frac{z_1}{c_1} v\sin\delta_\theta \\
&= -K_1\frac{s_1^2}{c_1} - K_2\frac{(\theta_e - \delta_\theta)^2}{c_2} - K_3\frac{(\psi_e - \delta_\psi)^2}{c_3} - \frac{\theta_a}{c_1}\frac{y_1^2}{|y_1| + d_1} v\cos\theta_e - \frac{\psi_a}{c_1}\frac{z_1^2}{|z_1| + d_2} v < 0
\end{aligned} \tag{18}$$

thus proving attractivity to the path for any initial condition that guarantees that $|\theta_e| < \frac{\pi}{2}$ for all *t*.

IV. TIME-CRITICAL COORDINATION

Having solved the problem of path following for a single vehicle and an arbitrary speed profile, we now address a very general problem of time-critical coordination of multiple vehicles. Examples include the situations where all vehicles must arrive at their final destinations at exactly the same time, or at different times so as to meet a desired inter-vehicle arrival schedule. Without loss of generality we consider the problem of simultaneous arrival. Let t_f be the common arrival time and define $\tau_i' = \frac{\tau_i}{\tau_{fi}}$. Clearly, $\tau_i'(t_f) = 1$, i=1,2,…,n implies that all vehicles arrived at their final destinations at the same time. From the definition of τ_i' it follows that $\dot{\tau}_i' = \frac{\dot{\tau}_i}{\tau_{fi}}$. Therefore, from (16) we obtain

$$\dot{\tau}_i' = \frac{K_1 s_{1i} + v_i\cos\theta_{e,i}\cos\psi_{e,i}}{\tau_{fi}} = \frac{v_i}{\tau_{fi}} + \frac{d_i}{\tau_{fi}}, \tag{19}$$

where $d_i = K_1 s_{1i} + v_i(\cos\theta_{e,i}\cos\psi_{e,i} - 1)$. Note that if the path following problem is solved, then $d_i \to 0$, *as* $t \to \infty$. This suggests that the simplified coordination dynamics be written as

$$\dot{\tau}' = u, \tag{20}$$

where *u* represents a scaled vector of velocity control inputs that are used to achieve time-critical coordination.

To account for the communication constraints we borrow from algebraic graph theory. See for example [19, 20] for an

introduction to the subject and [18] for an application to coordinated motion control. To this effect, let L denote the Laplacian of a connected undirected graph Γ that captures the underlying bidirectional communication network of the UAV formation (in particular the graph specifies, for each vehicle, what vehicles it exchanges information with). It is well known that $L \in R^{n\times n}$, $L \geq 0$, *rank(L)=n-1* and $L1_n = 0$ [20]. Therefore, there exists a positive definite diagonal matrix L_{11} with the nonzero eigenvalues of L on the diagonal and an orthonormal matrix $U \in R^{n\times(n-1)}$, $rank(U) = n-1$ such that

$$\begin{bmatrix} \frac{1_n}{\sqrt{n}} & U \end{bmatrix}^T L \begin{bmatrix} \frac{1_n}{\sqrt{n}} & U \end{bmatrix} = \begin{bmatrix} 0 & 0 \\ 0 & L_{11} \end{bmatrix}, \quad (21)$$
$$U^T 1_n = 0,\ U^T U = I, UL_{11}U^T = L.$$

Motivated by the analysis in [18] define the error vector $\mu = U^T \tau'$. Then from (14) it follows that $\mu = 0 \Leftrightarrow \tau_1' = \tau_2' = ... = \tau_n'$. This is well known in the literature on cooperative control as an Agreement Problem (see for example [21, 22]). Clearly,

$$\dot{\mu} = U^T u \quad (22)$$

Using this set-up, the general coordination problem addressed in this paper is formally stated next.

Problem 2 (Coordination) *Consider the coordination system with simplified dynamics (22). Suppose that each UAV exchanges its coordination parameter τ_i' with its neighbors, according to the topology of the communications network, as expressed in terms of the connected undirected graph Γ. Elect vehicle 1 as the formation leader and let $v_{d,1}$ denote its desired speed profile. Determine a control law for u such that $\tau_1' = \tau_2' = ... = \tau_n'$ = 1 at final time t=t_f.*

Remark 2 The above formulation leads to an inherently finite time horizon problem, In this paper, we solve it indirectly by using asymptotic stability results. Following common practice, this can only be done approximately by judicious choice of the control gains and initial conditions. The following proposition solves this simplified coordination problem. A similar formulation is used in [18] to address the coordination of mobile robots.

Proposition 2 *The control law*

$$u = aL\tau' + \begin{bmatrix} \frac{v_{d,1}}{\tau_{f1}} \\ \chi_I \end{bmatrix} = C_1^T \left(\frac{v_{d,1}}{\tau_{f1}} + aC_1 L\tau' \right) + C_2^T (aC_2 L\tau' + \chi_I) \quad (23)$$

$$\dot{\chi}_I = cC_2 L\tau',$$

where a and c are negative scalars and $\begin{bmatrix} C_1 \\ C_2 \end{bmatrix} := \begin{bmatrix} 1 & 0_{n-1}^T \\ 0_{n-1} & I_{(n-1)\times(n-1)} \end{bmatrix}$ *solves the simplified coordination problem.*

Remark 3 The control law (16) has a Proportional-Integral (PI) structure, thus allowing each vehicle to learn the speed of the leader, rather than having it available a priory. In fact, if $v_{d,1}$ is constant and the coordination control system is stable then, as shown later, the steady state value of the integrators x_{Ii} is $\frac{v_{d,1}}{\tau_{f1}} 1_{n-1}$. In scalar form, the control law u can be written as

$$\begin{aligned} u_1 &= \frac{v_{d,1}}{\tau_{f1}} + \sum_{j\in J_1} a(\tau_1' - \tau_j'), \\ u_i &= \sum_{j\in J_i} a(\tau_1' - \tau_j') + x_{Ii}, \\ \dot{x}_{Ii} &= \sum_{j\in J_i} c(\tau_1' - \tau_j'); i = 2,...,n, \end{aligned} \quad (24)$$

where J_i denotes the set of neighboring vehicles that vehicle i is allowed to communicate with. Clearly, this implementation meets the communication constraints addressed in the coordination problem formulation. Notice also how the gains a and c play the role of tuning knobs to adjust the speed of convergence of the coordination error μ to 0. This is important, in view of the comments in Remark 2.

Proof of Proposition 2. The feedback system consisting of (22) and (23) can be written as

$$\begin{aligned} \dot{\chi}_I &= cC_2 UL_{11}\mu \\ \dot{\mu} &= aL_{11}\mu + U^T \left(C_1^T \frac{v_{d,1}}{\tau_{f1}} + C_2^T \chi_I \right), \end{aligned} \quad (25)$$

where we used the fact that $L = UL_{11}U^T$. Assuming $v_{d,1}$ is fixed, the only equilibrium point $\begin{pmatrix} \mu_0 & \chi_{I0} \end{pmatrix}$ of (25) is the solution to

$$0 = cC_2 UL_{11}\mu_0, \quad 0 = aL_{11}\mu_0 + U^T (C_1^T \frac{v_{d,1}}{\tau_{f1}} + C_2^T \chi_{I0}). \quad (26)$$

From the first expression in (26), and using the fact that $C_2 U$ is full rank (see Lemma 1) we obtain

$$\begin{aligned} &0 = \mu_0 \Rightarrow 0 = U^T (C_1^T \frac{v_{d,1}}{\tau_{f1}} + C_2^T \chi_{I0}) \Rightarrow \\ &0 = U^T \begin{bmatrix} \frac{v_{d,1}}{\tau_{f1}} \\ \chi_{I0,1} \end{bmatrix} \Rightarrow \chi_{I0} = \frac{v_{d,1}}{\tau_{f1}} 1_{n-1}, \end{aligned} \quad (27)$$

since $U^T 1_n = 0$.

Next, we address the stability of the above equilibrium point. To this effect, we compute the eigenvalues of the state matrix associated with (25), that is, the solutions of

$$\begin{aligned} &\det \begin{bmatrix} \lambda I & -cC_2 UL_{11} \\ -U^T C_2^T & \lambda I - aL_{11} \end{bmatrix} = 0 \Rightarrow \\ &\det(\lambda I (\lambda I - aL_{11}) - cU^T C_2^T C_2 UL_{11}) = \\ &\det(\lambda^2 L_{11}^{-1} - a\lambda I - cU^T C_2^T C_2 U) = 0, \end{aligned} \quad (28)$$

where we exploited the result that for any compatible square matrices $A,\ B,\ C,\ D$ $\det \begin{bmatrix} A & B \\ C & D \end{bmatrix} = \det(AD - CB)$, if $AC = CA$ [23].

It now follows, using Lemmas 1 and 2 in the Appendix, that the roots λ in (28) have negative real parts for any negative scalar gains a and c, thus proving stability.

V. SIMULATIONS

As explained before, the nonlinear path following and coordination algorithms derived in Section III and IV rely on a kinematic model of the vehicle under consideration. The final control law manipulates directly pitch and yaw rate, which should be viewed as virtual control commands issued by the outer loop in an inner-outer control architecture. An inner loop must be designed at a later stage to actually generate the required pitch and yaw rate commands. This problem will not be addressed here. Instead, we assume that an inner loop autopilot is available that yields adequate performance.

Control commands generated by (10) and (16) were used to drive a model of the inner loop autopilot that is actually implemented on-board the Telemaster UAV used at NPS (wing span 2.5m, take-off weight 8kg), as shown in Fig.5.

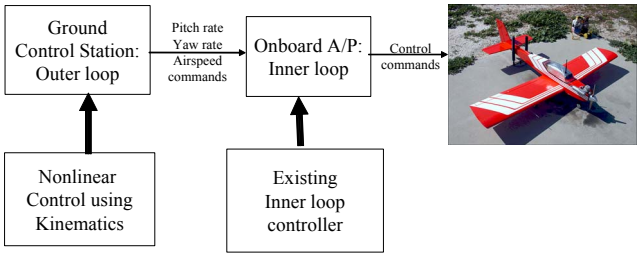

Fig.5. Inner/outer control structure.

The nonlinear 6DOF simulation of three Telemasters executing the coordinated time-critical path following maneuver presented in Fig.1 was implemented in Simulink. The underlying communications network was modeled using an undirected graph shown in Fig.6, where a vertex represents an UAV and an edge a bidirectional link between two vertices.

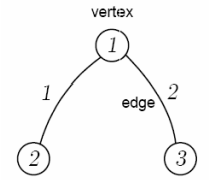

Fig.6. Undirected graph that models the structure of the bidirectional network used in the simulation.

Figure 7 shows the spatially deconflicted trajectories followed by each UAV from right to left. The triangles indicate the location of each vehicle along its path at 20 sec intervals and the circles represent the location of each UAV at the time instant the 1st UAV arrived at its destination. Clearly all three UAVs have arrived almost simultaneously.

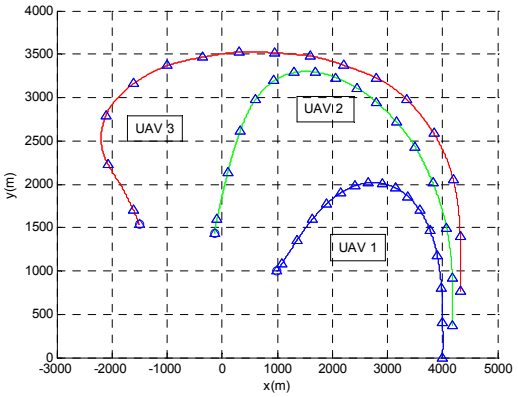

Fig.7. Time coordinated maneuver by a formation of three UAVs.

Figure 8 shows the path following errors for each UAV during the maneuver. The errors in y and z channels are very small for UAV 1 and increase for UAVs 2 and 3 as the trajectories get more aggressive. This behavior can in principle be improved by proper re-design of the inner loop systems. Nevertheless, these results demonstrate a proof of concept. Notice that the values for s_1 vary significantly; however, by design this has no impact on performance.

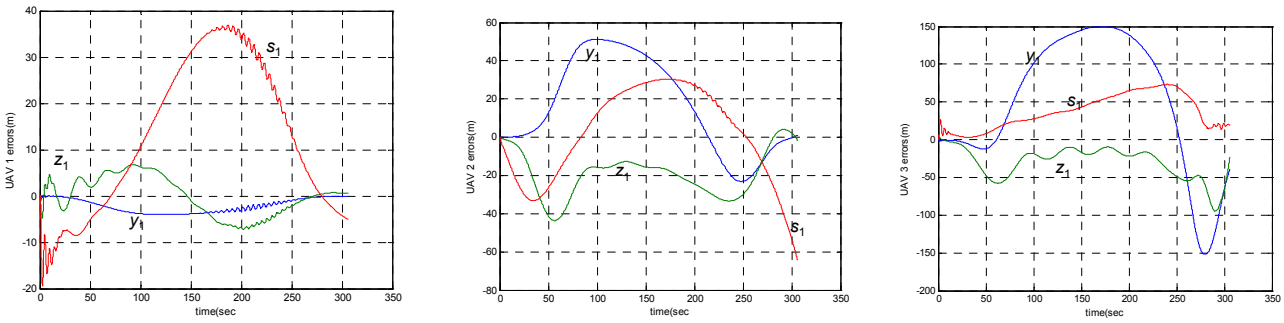

Fig.8. Time coordinated maneuver – path following errors.

VI. CONCLUSIONS

The paper described a novel solution to the problem of coordinated control of multiple unmanned air vehicle (UAV) to ensure collision-free maneuvers under strict spatial and temporal constraints. Both theoretical and simulation results were presented. The theoretical results showed convergence of the path following and time-critical coordination algorithms developed. The simulations results have shown that the algorithms proposed hold potential for future real applications.

REFERENCES

[1] R. Beard, L. Lawton, F. Hadaegh, "A coordination architecture for spacecraft formation Control," *IEEE Trans. Contr. Systems Technology*, vol. 9, pp. 777-790, 2001.

[2] F. Giuletti, L. Pollini, M. Innocenti, "Autonomous formation flight," IEEE *Control Systems Magazine*, vol. 20, pp.34–44, 2000.
[3] Pratcher, J. D'Azzo, A. Proud, "Tight formation control," *Journal of Guidance, Control and Dynamics*, 24(**2**), 2001, pp.246-254.
[4] M. Queiroz, V. Kapila, Q. Yan, "Adaptive nonlinear control of multiple spacecraft formation flying," *Journal of Guidance, Control and Dynamics,* 23(**3**), 2000, pp.385-390.
[5] D. Soetanto, L. Lapierre, A, Pascoal, "*Adaptive non-singular path following control of dynamic wheeled robots,*" Proc. ICAR'03, Coimbra, Portugal.
[6] P. Ogren, M. Egerstedt, X. Hu, "A control Lyapunov function approach to multiagent Coordination," *IEEE Trans. on Robotics and Automation,* 18, 2002.
[7] P. Encarnação, A. Pascoal, "Combined trajectory tracking and path following: an application to the coordinated control of marine craft," IEEE Conf. Decision and Control, Orlando, Florida, 2001.
[8] L. Lapierre, D. Soetanto, A. Pascoal, "Coordinated motion control of marine robots," *Proc. 6th IFAC Conference on Maneuvering and Control of Marine Craft (MCMC2003)*, Girona, Spain, 2003.
[9] R. Skjetne, I. Flakstad, T. Fossen, "Formation control by synchronizing multiple maneuvering Systems," *Proc. 6th IFAC Conference on Maneuvering and Control of Marine Craft (MCMC2003),* Girona, Spain, 2003.
[10] D. Stilwell, B. Bishop, "Platoons of underwater vehicles," *IEEE Control Systems Magazine*, December, 2000, pp.45-52.
[11] O. Yakimenko, "Direct method for rapid prototyping of near-optimal aircraft trajectories," *AIAA Journal of Guidance, Control, and Dynamics,* 23(**5**), 2000, pp.865-875.
[12] A. Neljubov, "Mathematical methods of air vehicle with thrust vector turn possibility battle, takeoff and landing maneuvers calculation," *Air Force Engineering Academy Press*, Moscow, 1986.
[13] V. Taranenko, "Experience of Ritz's, Puankare's and Ljapunov's methods utilization for flight dynamics tasks solution," *Air Force Engineering Academy Press*, Moscow, 1986.
[14] V. Taranenko, V. Momdgi, "Direct variational method in boundary tasks of flight dynamics," *Mashinostroenie*, Moscow, 1986.
[15] A. Micaelli, C. Samson, "Trajectory-tracking for unicycle - type and two - steering - wheels mobile robots," *Technical Report No. 2097, INRIA,* Sophia-Antipolis, France, 1993.
[16] I. Kaminer, A. M. Pascoal, E. Hallberg, and C. Silvestre, "Trajectory Tracking for Autonomous Vehicles: An Integrated Approach to Guidance and Control," of *AIAA Journal of Guidance, Control and Dynamics*, 21(**1**), 1998 pp.29-38.
[17] P. Encarnação, A. Pascoal, "3-D Path Following for Autonomous Underwater Vehicles," *Proc. 39th IEEE Conference on Decision and Control*, Sydney, Australia, 2000.
[18] R. Ghabcheloo, A. Pascoal, C. Silvestre and I. Kaminer, "Nonlinear Coordinated Path Following Control of Multiple Wheeled Robots with Bidirectional Communication Constraints," *submitted for publication to Journal of Adaptive Control and Signal Processing*.
[19] Biggs N, Algebraic Graph Theory, (2nd Edition) *Cambridge University Press, 1993.*
[20] Godsil C, and Royle, Algebraic Graph Theory, *Springer-Verlag, 2001*.
[21] J. A. Fax, and R. M. Murray, "*Information flow and cooperative control of vehicle formations*," IEEE Transactions on Automatic Control, 49(**9**), 2004, pp.1465-1476.
[22] A. Jadbabaie, J. Lin, and A. S. Morse, "*Coordination of groups of mobile autonomous agents using nearest neighbour rules*," IEEE Transactions on Automatic Control, 48(**6**), 2003, pp.988–1001.
[23] Horn R.A. and Johnson C. R., Matrix Analysis, *Cambridge University Press*, 1985.

APPENDIX

Lemma 1. *The matrix* $C_2U \in R^{(n-1)X(n-1)}$ *has rank n-1.*

Proof. From the definition of C_2 it follows that C_2U consists of the last *n-1* rows of *U*. Suppose $\exists x$ such that $x^T C_2 U = 0$ Let $x_1 = \begin{bmatrix} 0 & x^T \end{bmatrix}^T$. Since $x^T C_2 = x_1^T$ we obtain that $x_1^T U = 0$ which contradicts the fact that $1_n^T U = 0$ and 1_n is the only kernel (of *U*) (see expression (21)).

Lemma 2. *Let A, B, C be positive definite matrices of compatible dimensions. Then the roots of* $\det(\lambda^2 A + B\lambda + C) = 0$ *have negative real parts*.

Proof: (By contradiction) Suppose the results does not hold true. Then, either 1) $\mathrm{Re}(\lambda) = 0$ or 2) $\mathrm{Re}(\lambda) > 0$.

Case 1. Let $\lambda = j\omega$ for some $\omega \in R, \omega \neq 0$. Then $\det(\lambda^2 A + B\lambda + C) = 0$ implies that there exists a non-zero vector $p = p_1 + jp_2$ of compatible dimension such that

$$(\lambda^2 A + B\lambda + C)p = 0 \Rightarrow \left(-\omega^2 A + C\right)p_1 - B\omega p_2 = 0 \text{ and } \left(-\omega^2 A + C\right)p_2 + B\omega p_1 = 0 \Rightarrow$$

$$\Rightarrow p_2^T \left(-\omega^2 A + C\right)p_1 - p_2^T B\omega p_2 = 0 \text{ and } p_1^T \left(-\omega^2 A + C\right)p_2 + p_1^T B\omega p_1 = 0 \Rightarrow p_2^T B p_2 + p_1^T B p_1 = 0$$

On the other hand, if $\omega = 0,$ we obtain that $p^* C p = 0$.

Case 2. Let $\lambda = \alpha + j\omega, \alpha > 0, \omega > 0$. Then following the argument above there exists a non-zero vector $p = p_1 + jp_2$ such that

$$\left(\left(\alpha^2 - \omega^2\right)A + \alpha B + C\right)p_1 - \left(2\alpha\omega A + B\omega\right)p_2 = 0 \text{ and } \left(\left(\alpha^2 - \omega^2\right)A + \alpha B + C\right)p_2 + \left(2\alpha\omega A + B\omega\right)p_1 = 0$$

$$\Rightarrow p_2^T \left(2\alpha A + B\right)p_2 + p_1^T \left(2\alpha A + B\right)p_1 = 0$$

Similarly, if $\omega = 0,$ we obtain that $p^* \left(\alpha^2 A + \alpha B + C\right)p = 0$.